79-GT-53

inted in U.S.A.

an ASME publication

$3.00 PER COPY
$1.50 TO ASME MEMBERS

An Application of 3-D Viscous Flow Analysis to the Design of a Low-Aspect-Ratio Turbine

H. C. LIU

T. C. BOOTH

AiResearch Manufacturing Company of Arizona,
A Division of The Garrett Corporation,
Phoenix, Ariz.

W. A. TALL

United States Air Force,
Aero-Propulsion Laboratory,
Wright Patterson AFB, Ohio

Previously reported cascade test results verified and provided a calibration of the 3-D viscous flow analysis. This paper describes the subsequent AFAPL-sponsored technology program in which the 3-D viscous flow computer program was used to optimize the low-aspect-ratio stator of a high-work turbine stage. The optimization procedure, in conjunction with the radial distribution of energy extraction, led to innovative-but-realistic blading for advanced gas generator turbines. A turbine stage was tested with this stator, in conjunction with an appropriate rotor design. The total-to-total design-point efficiency — 92 percent at 1-percent tip clearance — was achieved at 31.83 Btu/lbm specific work. In addition to stage tests, separate stator tests were conducted including a measurement of total pressure loss and stator reaction torque, which provided baseline data to assess interaction effects during stage testing with stator reaction measurements "in vivo."

THE AMERICAN SOCIETY OF MECHANICAL ENGINEERS, UNITED ENGINEERING CENTER, 345 EAST 47th STREET, NEW YORK, N.Y. 10017

An Application of 3-D Viscous Flow Analysis to the Design of a Low-Aspect-Ratio Turbine

H. C. LIU   T. C. BOOTH   W. A. TALL

ABSTRACT

Previously reported cascade test results[4] verified and provided a calibration of the 3-D viscous flow analysis. This paper describes the subsequent AFAPL-sponsored technology program in which the 3-D viscous flow computer program was used to optimize the low-aspect-ratio stator of a high-work turbine stage. The optimization procedure, in conjunction with the radial distribution of energy extraction, led to innovative-but-realistic blading for advanced gas generator turbines. A turbine stage was tested with this stator, in conjunction with an appropriate rotor design. The total-to-total design-point efficiency -- 92 percent at 1-percent tip clearance -- was achieved at 31.83 Btu/lbm specific work. In addition to stage tests, separate stator tests were conducted including a measurement of total pressure loss and stator reaction torque, which provided baseline data to assess interaction effects during stage testing with stator reaction measurements "in vivo".

NOMENCLATURE

a'_{cr} = absolute critical speed of sound, m/sec, (ft/sec)

h = specific enthalpy, J/kg, (Btu/lbm)

i = incidence angle, deg.

N = rotational speed, rpm

P = absolute pressure, N/cm^2, $(lbf/in.^2)$

P_R = pressure ratio

R = radius, cm, (in.)

T = absolute temperature, deg K, (deg R)

V = absolute velocity, m/sec, (ft/sec)

W = relative velocity, m/sec, (ft/sec)

$\dot{W}$ = mass flow rate, kg/sec, (lbm/sec)

α = absolute gas flow angle measured from axial direction, deg

β = relative gas flow angle measured from axial direction, deg

γ = ratio of specific heats

Δ = increment

δ = ratio of inlet total pressure to U.S. standard sea-level pressure

ϵ = function of γ used in relating parameters to those using air inlet conditions at U.S. standard sea-level conditions.

$\bar{\epsilon}$ = kinetic energy loss coefficient, $1 - \dfrac{V^2}{V^2_{id}}$

η = efficiency

θ_{cr} = squared ratio of critical velocity at turbine inlet temperature to critical velocity at U.S. standard sea-level temperature.

$\bar{\omega}$ = total pressure loss coefficient, $\bar{\omega} = (P'_{in} - P')/(P'_{in} - P)$, P' and P are the local total and static pressures, respectively.

1

Subscripts

cr = condition corresponding to Mach number of unity

id = ideal

in = inlet

T-T = Total-To-Total

x = axial component

u = tangential component

1 = station at stator inlet

2 = station at rotor inlet

3 = station at rotor exit

Superscripts

' = absolute total state

" = relative total state

I. INTRODUCTION

The development of low-aspect-ratio turbine (LART) technology has been an important aspect of AiResearch R&D efforts for several years. The LART Program evolved primarily from annular divergence studies of an in-house R&D turbine program[1] and the parallel development of a 3-D computer solution to the Navier-Stokes equations[2]. The objectives of this program were to investigate secondary flow phenomena pertinent to low-aspect-ratio blading, and develop a design-system for such blading based on newly-developed computer programs.

While Phase I[3,4] of the LART Program focused on calibration of the 3-D flow computer program, Phase II was a direct application of this program to the design optimization of a low-aspect-ratio stator. The stator was tested both alone and as part of a stage.

An extensive test gave both basic performance information and a better understanding of the flow mechanisms within the turbine. In addition to extensive stator and rotor exit surveys, a stator reaction mechanism was designed into the rig to measure stator torque in the presence of a rotor, thus allowing stator-rotor interaction effects to be measured.

II. TURBINE DESIGN AND VELOCITY DIAGRAMS

The turbine design point was selected for an advanced gas generator cycle. The rotational speed of 24,863 rpm was derived from a design-point trade-off study, in which realistic cooling flow, blade life, disk bore, and allowable stresses were imposed as mechanical design constraints. Other pertinent turbine design parameters are listed in Table 1.

The concept of radially distributing the stage energy extraction to minimize end-wall effects was the key element in the velocity diagram optimization. The velocity diagram was selected on the basis of the measured stator loss distribution from the Phase I cascade tests. The resulting stator exit angle distribution is shown in Figure 1. An equivalent free-vortex angle distribution is shown for reference.

The other important part of the velocity diagram optimization was rotor reaction. Since the rotor-exit condi-

2

tion affects the downstream losses, the optimization included consideration of an interstage duct and downstream stator with both co-rotating and counter-rotating LP turbine configurations. Results showed that, for either co-rotation or counter-rotation, the higher hub reaction configuration yielded higher overall efficiency until the downstream losses for the duct and the high turning of the co-rotating stator became dominant. The rotor-hub reaction selected was 27 percent. The velocity diagrams for the tip, hub, and 50-percent streamline are shown in Figure 2.

III. STATOR DESIGN OPTIMIZATION

A conventional two-dimensional airfoil design and analysis was performed to evaluate the solidity requirement, vane loading, and possible underturning. Two stators, identified as Models IIA and IIB and differing primarily by solidity (IIB has a reduced axial chord), were designed and analyzed. The solidity of the Model IIA stator was selected using the incompressible Zweifel tangential loading criterion, which is derived from 2-D cascade testing. The Model IIA stator was designed with a midspan value for the Zweifel loading coefficient of 0.859, whereas the Model IIB stator was designed with a Zweifel loading coefficient of 0.932. Both vanes, which were designed with 9 degrees of downstream turning, have an acceptable loading. (The profiles and theoretical loading distributions are given in Reference 3.) However, these 2-D results alone were not used for making a design selection. The 3-D viscous analysis techniques were applied both to select a final profile and to evaluate the effects of end-wall contour and vane-stack for reducing the secondary flow and associated losses.

The Phase II stator design drew upon the prior testing and analysis of Phase I, but also recognized the effects of reduced end-wall solidity and vane-profile lean. During Phase I, radial distribution of flow was shown to have an influence on end-wall flows in low-aspect-ratio stators where a relatively uniform radial distribution of flow was achieved. This is contrary to what would be expected from an analysis of the stator-parabolic-exit angle distribution with radially constant losses. In that instance, flow would be increased on the end walls and reduced at the mid-span. Phase I test results indicated and the subsequent 3-D viscous analysis confirmed that, due to the higher end-wall losses, the parabolic-stator angle distribution compensated for the otherwise low end-wall flow conditions that would exist with linear stator-exit angle distribution. This factor results in a more uniform radial distribution of flow at the stator exit.

The following configurations, illustrated in Figure 3, were analyzed for the Model IIA stator. The first was a bellmouth shroud and hub contour (Type C1), with a baseline stack at the center of the throats. The second was an inflection shroud contour with an opened hub inlet (Type C2), with a baseline stack at the center of the throats. The third and final was a 20-degree leaned stack with the bellmouth end-wall contour (Type C1).

The effect of tangential lean on the radial distribution of losses is shown in Figure 4. In addition, data generated by Northern Research Engineering Corporation[5] which supports the predicted trends is shown.

Results of the Model IIA vane analysis show that the bellmouth contour has high losses from the hub to two-thirds of the vane span. The inflection contour reduces loss significantly across the span, except for the top 15 percent of the vane span. The leaned vane generates an inverse radial loss distribution from that of the baseline-stack vane with the same end-wall contours. The improvement at the hub region is offset by the increased losses at the tip region. The integrated losses for these three configurations are tabulated in Table 2 for comparison.

The strong effects of vane lean and end-wall contour were shown in analyses of the Model IIA stator; the impact of solidity on this optimization matrix was studied with 3-D flow analyses employing the Model IIB stator. However, to increase the stator reaction and reduce the losses, the stator-inlet area was increased utilizing a larger bellmouth end-wall contour designated as contour C3. The contours employed for the IIB studies are shown in Figure 5. The reduced chord of the Model IIB stator precluded the use of an inflection contour since the design philosophy was both to shape all contouring upstream of the throat and to avoid excessive flow path curvature.

The success of the dihedral in redistributing the losses suggested this to be an effective tool for shaping the three-dimensional flow. Therefore, borrowing from the single-axis lean in which tip end-wall flows were apparently concentrated at the tip, compound lean was investigated whereby the IIB vane was restacked by moving the mid-section tangentially so that the suction surface is concave at the trailing edge. The compound lean angle between the vane surface and a radial line is approximately 13.5 degrees, both at tip and hub. This lean combined with the C3 contour was analyzed.

Table 2 summarizes the integrated loss for the several vane configurations analyzed. It is immediately apparent that the low-solidity baseline case offers superior stagnation-pressure loss performance relative to the high-solidity vane with the same end-wall contour. Furthermore, the basic end-wall contour (C1) has a distinct advantage over the large bellmouth contour (C3) in terms of loss level. Radial loss distributions showed that the use of contour (C1) results in lower end-wall losses.

The compound lean effects also revealed an improvement in the loss distribution and level. The introduction of 13.5-degree compound lean resulted in a decrease in loss from 0.062 to 0.055. The mixed-out radial distribution of loss indicated a reduction at both end walls, which is consistent with the Model IIA stator results with a 20-degree vane lean in one direction. Therefore, to determine if a further shift in the stack might reduce the losses, a second restack of the Model IIB vane was defined with a compound lean of 26 degrees (configuration 4). In summary, the effects of the various stacks of the Model IIB vane are that increasing suction-surface concavity reduces losses near the end wall and increases mid-span losses, while maintaining the same overall loss. Since the 26-degree compound lean has both significantly lower end-wall losses and a relatively flat cross-passage loss profile, this stack configuration was chosen.

To determine the effect of end-wall bellmouth contouring on a compound-lean vane, configurations 5 and 6 were defined and analyzed. This comparison revealed that increased end-wall convergence (contour C3 has the greatest convergence) reduces end-wall losses. However, mid-span losses are increased to the extent that the overall loss remains essentially the same for all three contours. A bellmouth with an intermediate rate of convergence (contour C4) was finally analyzed with the full 26-degree compound lean. For this, configuration 7, the trend of reducing end-wall losses with increasing convergence is noticeable; however, a significant increase in mid-span losses was also noted. Consequently, contour (C1) was selected to combine with the Model IIB stator stacked with a 26-degree compound lean to form the final design of the Phase II stator.

The effects on the radial distribution of loss of end-wall contour, solidity, and compound lean are compared in Figures 6 and 7.

To summarize the design effort, three-dimensional viscous analyses of the Model IIA stator design (high end-wall solidity) with bellmouth and inflection-contoured end walls indicated that the inflection contour reduced average losses. However, end-wall losses remained high. The observation that radial components of vane force must affect radial flows in the vane-surface boundary layers suggested the need for investigation of the effects of vane lean on end-wall losses. Carter and Lenherr[5] tested leaned 2-D cascades wherein the hub suction-surface corner angle was increased beyond 90 degrees. These tests showed improved hub losses but increased tip losses. A similar lean (20 degrees) was incorporated in the Model IIA stator, and similar results were predicted by a 3-D viscous analysis. Thus, vane lean was shown to have an important effect on end-wall losses.

In order to determine the effect of end-wall solidity on end-wall losses, the Model IIB stator was designed and analyzed with the configuration 1 end wall without lean. This design achieved lower overall losses compared with the high end-wall solidity vane on the Model IIA stator. Increased end-wall convergence, applied to the Model IIB stator vane, resulted in increased losses.

To further improve loss distributions of the Model IIB stator vane, it was observed that, due to the parabolic-exit angle distribution, a compound lean could be introduced into the Model IIB stator vane. A compound lean would tend to force vane boundary-layer flows to a mid-span position, thereby reducing end-wall loss gradients. This lean is achieved by stacking the Model IIB stator-vane sections on a radial line upstream of the trailing edge. This results in a hub lean angle similar to the Model IIA stator configuration, but with an opposite lean at the shroud. Analysis of this configuration confirmed the expected reduction of end-wall losses. An increase in compound lean resulted in a further loss reduction, and achieved uniform flow over 80 percent of the vane-exit span. Fillipov, et al,[6] published test results showing similar compound-lean effects on vane end-wall losses which adds confidence to the validity of the computed results.

IV. ROTOR DESIGN

The rotor blade design for a high-work turbine deserves at least as much attention as the stator vane, since the three-dimensional flow field is considerably more complex than that of the stator. There are several reasons for the added complexity. First, rotor inlet conditions are affected by the 3-D flow from the stator, which appears unsteady in the relative frame-of-reference due to tangential nonuniformity. Second, the rotating frame-of-reference imparts centrifugal and Coriolis forces that affect the flow distribution. Finally, for an unshrouded rotor, the flow disturbances due to the tip leakage cannot yet be predicted. None of these effects are currently taken into account in the 3-D viscous flow analysis, so the rotor was designed using conventional techniques -- i.e., a design procedure based on an iterative application of an axisymmetric analysis and the blade-to-blade analysis.

For a cooled, high-work rotor blade, the tendency to decrease the aspect ratio and reduce solidity is inevitable just as for the stator. The Phase II rotor design, however, was not intended to establish the trade-offs or the limits of these two important geometrical parameters. Instead, Phase II design aspect ratio and solidity levels were selected based on current technology and in-house design experience.

V. TEST APPARATUS

Instrumentation for the rig was designed both to measure basic stage performance with Kiel probes, thermocouples, a sonic nozzle, dynamometer, and shaft torque-

3

meter and to supply fundamental aerodynamic data including stator- and rotor-exit surveys, flow-path pressure distribution, and vane pressure distribution. The stator test configuration was accomplished with the turbine rotor removed and a pressure-rake carrier installed. The carrier was equipped with an indexing mechanism which permitted the twenty-one element total-pressure rake to traverse one and one-half vane passages at 0.5-degree increments.

VI. STATOR PERFORMANCE

Stator performance was ascertained from circumferential surveys with a twenty-one element total-pressure rake (mounted in the rotor leading-edge location) and three conventional radial surveys. The rake data was used to generate contour plots (illustrated in Figure 8) to interpret radial survey results by superimposing the survey locations, and to provide circumferentially-averaged loss distributions and overall integrated loss information.

The three cobra-survey probes were located in three different passages. These positions were translated to a single stator passage, as shown in Figure 8, which shows the traverse location superimposed on a contour plot of total-pressure loss. This composite figure clearly demonstrates the need for multiple-probe surveys in conducting stator exit measurements. The stator wakes are strongly curved, so that a single probe traverse does not remain in a flow wake pattern.

A summary of calculated and measured stator performance is given in Table 3. To show the technical progress achieved in the new design, analytical predictions from the 3-D viscous analysis and data from the LART Phase I Model D stator are also presented in the table. Note that the optimization at low Mach numbers focused on a uniform loss distribution. However, at high Mach numbers, a reduction of from 0.0636 to 0.0586 was achieved.

Comparing Phase II loss contours with Phase I data as illustrated in Figure 9, it was found that the Phase II stator flow is much cleaner at the end walls. This showed that the design objective was met, since an attempt was made to reduce both the end-wall secondary flow and the surface boundary-layer flow accumulation at the end walls. In this way, stator-exit flow uniformity was enhanced to improve rotor performance.

Radial distributions of the total pressure-loss coefficient, $\bar{\omega}$, are given in Figure 10. For comparison, the analytical prediction for the $\bar{\omega}$ distribution is also presented. A comparison of experimental radial distributions of loss reveals that a loss peak occurs at about 75-percent span at the lower Mach number, and moves to the 47-percent span position at the higher Mach number. This shift was presumably due to a larger radial pressure gradient, forcing the losses to mid-span at the high Mach number. However, at high Mach number, the design objective of a flat loss distribution was achieved.

Vane surface static pressure distributions were also measured during Phase II testing. The subsonic distributions, given in Reference 3, compare favorably with the analysis completed with the subsonic 3-D viscous flow analysis. Predictions of the design-point pressure distributions were presented subsequently by Dodge[4] in the final report of the AFAPL-sponsored program in which compressibility effects were added to the 3-D flow analysis.

VII. STAGE PERFORMANCE

Turbine work was measured by both the temperature drop and the shaft torque. The turbine performance is rated in terms of temperature drop. However, the work output was computed by both methods, each serving as a check on the other. Measurement of exit total pressure was complicated by the highly-curved stator wakes. Therefore, a contour map of the rotor-exit total-pressure field was generated from a composite of Kiel probe data at the rotor exit and the two cobra- probe surveys. All data points were translated to a single vane spacing from which a contour plot was synthesized. Computed rotor-exit total pressures were found by area-averaging the contour plots. This analysis, carried out at the design point, verified the Kiel probe data, which was subsequently used alone to rate off-design turbine performance.

The design point efficiency for the LART stage is 0.920. Stage performance obtained during Phase II of the LART program is summarized in Table 4. At the design pressure ratio, the turbine exhibited an optimum efficiency level at 100- and 110-percent speeds. However, at 90-percent speed, the efficiency is 2.4 points lower than at the design speed due to the increased positive incidence in conjunction with a higher-than-design inlet relative Mach number. This is a typical condition for the hub region of a high-work rotor with both a thick leading edge for internal cooling and a high inlet relative Mach number. Under these conditions, blade blockage at the beginning of the guided channel drives the suction-surface Mach number to an excessive level where it is followed by a shock and associated separated boundary-layer losses. Such a situation was anticipated during the design phase. Even at the design condition, where the incidence and inlet relative Mach number were lower, the calculated loading was extremely sensitive to the leading-edge geometry.

VIII. TORQUE MEASUREMENTS

Phase II of the LART program applied the analytical and design methods, developed in Phase I, to the design of a low-aspect-ratio turbine stage. Progress was demonstrated through both a stator and a stage test. Since the program stressed stator design, it was particularly important to assess stator performance. To this end, the stator was installed in the test rig so that its reaction torque could be measured during testing. The obvious benefit of such a measurement is to subsequently establish stator effects on performance when rotor is in place.

The test objective was to relate, with and without the rotor, the stator expansion ratio to the angular momentum imparted by the stator to the fluid. Measured torque values were incorporated into an analysis that gave stator-exit mean-velocity diagrams and losses. A mean-line velocity diagram at stator exit was determined from corrected torque, corrected flow, stator-exit pressure, and various geometric information.

The measurements were accomplished by suspending the stator assembly from four elastic beams, and measuring the beam stress field with strain gauges during operation. The strains were correlated with stator torque by use of a dead-weight calibration test. To ensure that the stator was freely suspended and not touching any adjacent rig part, outside-inside air sealing was accomplished by an air-buffered labyrinth seal arrangement. The entire stator assembly was electrically isolated from the main portion of the rig, thereby permitting friction-producing mechanical contact to be detected by use of an ohmmeter. To eliminate thermal effects, the strain gauges were temperature compensated with respect to the beam material, and cooling air was directed over them to minimize any temperature gradients. Due to interaction of axial and twisting loads on the beam deformations, the gauges were positioned to measure each type of deformation.

Torque measurements were recorded during a baseline stator-only test. The corrected torque for each expansion ratio was numerically averaged over several data scans, and

4

a torque curve was generated. As a check on the measured results, the torque was calculated from the data measured at the design pressure ratio with the three stator-survey probes. The calculated corrected torque was within 0.5 percent of the measured corrected torque.

To obtain a meanline velocity diagram from the torque and flow data, the stator exit static pressure must be determined. Analysis reveals that the stator total-pressure losses are very sensitive to the number selected to represent the stator-exit static pressure, which is extremely non-uniform. Moreover, the stator- exit pressure distribution varied during the testing, making it difficult to select a single number typifying the pressure distribution. For example, circumferential pressure distributions for the stator end walls at the trailing edge for the design-point condition measured during the stage and stator tests are shown in Figure 11. For comparison, the downstream (tip) reference static pressure ratio is also included in the figure (This reference pressure was measured on the stator tip just downstream of the trailing edge on a central "streamline"). The presence of the rotor is clearly seen; the reference tap data suggests the stator "exit pressure" is the same with or without the rotor. The distribution clearly shows an effect of the rotor on the flow.

It is clear that no single pressure tap gives a pressure representative of the stator-exit pressure distribution. Several schemes for picking a static-pressure value were explored; these included scaling the pressure from a single pressure tap, using the unscaled pressure from a single tap, and area-averaging the static pressures. Each technique was used to generate performance data for the stator-only test and compared with the results of the rake survey. An analysis of the velocity diagrams, derived from the torque data, was conducted over the range of tested pressure ratios from the stator testing. The total-pressure results are presented in Figure 12. The area-averaged pressure technique yielded an accurate loss value at the survey pressure ratio. Moreover, it was later found that a similar definition for the hub and shroud end-wall static pressure led to an axisymmetric simulation of the test points consistent with the torque analysis. The results of the torque analysis are given in Table 5 along with results of the axisymmetric analysis.

The philosophy adopted for the axisymmetric analysis was to match inlet conditions, rotor exit surveys, stator-exit static pressure values, and the total pressure loss distribution. The level of the loss distribution was adjusted to match the stator-exit stator pressure. Such a procedure led to stator and rotor loss coefficients ($\bar{\omega}$) of 0.0650 and 0.1486 respectively.

IX. SUMMARY AND CONCLUSIONS

The primary objective of the LART Program has been to develop new design methods for low-aspect-ratio turbines, the performance of which has previously been degraded by end-wall secondary flows.[8] The approach taken was to use newly developed analytical tools.

Phase II of the program, was an application of the analytical tools calibrated with cascade data in Phase I to design a high-work, low-aspect-ratio turbine. The success of the approach is measured by the 92-percent total-to-total design-point efficiency achieved in the test. An important element contributing to the high stage efficiency is the stator design; its end-wall shape, solidity, and stacking configuration were optimized with the three-dimensional viscous flow analysis. The Phase II stator achieved a design-point total-pressure-loss coefficient, $\bar{\omega}$, of

0.059. The technical progress may be measured by comparison with the Phase I stator which was designed with a similar velocity diagram and achieved a performance level of 0.064.

Program Conclusions

o The three-dimensional viscous flow analysis has demonstrated capability to predict performance changes properly in response to geometric changes.

o A parabolic turning distribution in conjunction with a properly contoured and stacked stator can produce a low-loss stator with a uniform loss distribution. Application of this principle led to excellent stage performance in Phase II of the LART program.

o Stator solidity, established on the basis of a two-dimensional loading criterion, may be reduced with decreased overall stator loss. This is illustrated by the LART Phase II design, in which the average solidity was reduced by 8 percent and the overall loss was decreased by 22 percent, based on three-dimensional analysis results.

o The feasibility of measuring stator reaction torque has been demonstrated. The technique is believed to have sufficient sensitivity to detect interaction effects.

X. ACKNOWLEDGEMENTS

XI. REFERENCES

1 Schlegel, J. C., Liu, H. C., and Waterman, W. F., "Reduction of End-Wall Effects in a Small, Low-Aspect-Ratio Turbine by Radial Work Redistribution," Paper No. 75-GT-7 presented at ASME Gas Turbine Conference, Houston, Texas; March 1975.

2 Dodge, P. R., "A Numerical Method for 2-D and 3-D Viscous Flows," AIAA Paper No. 76-425.

3 AFAPL Low-Aspect-Ratio Turbine Technology Program, Phase I Final Report, Contract No. F33615-74-C-2017, August 31, 1975.

4 Waterman, W. F., and Tall, W.A., "Measurement and Prediction of 3-D Viscous Flows in Low-Aspect-Ratio Turbine Nozzles," ASME Paper No. 76-GT-73, presented at ASME Gas Turbine Conference, New Orleans, Louisiana, March 1976.

5 Carter, A. F., and Lenherr, F. K., "An Investigation of Efficiency Limits for Small Cooled Turbines," USAAVLABS Technical Report 70-14, August, 1970.

6 Fillipov, B. A., and Van Chzhun-TSI, "The Effect of Flow Twisting on the Characteristics of Guide Rows," Teploenergetika, 1964, 11, 5, 54-57.

7 AFAPL 3-D Heat Transfer Analysis Program, USAF Final Report No. AFAPL-TR-77-64, October, 1977.

8 Tall, W. A., "Understanding Turbine Secondary Flow," Paper No. 14, 49th Meeting of Propulsions, Energetics and Power Panel, AGARD, March 1977.

TABLE 1. TURBINE DESIGN POINT.

$$P_{in} = 116.4 \text{ psia} \quad (80.255 \text{ N/cm}^2)$$

$$T_{in} = 2960^\circ R \quad (1644^\circ K)$$

$$P_{R_{T-T}} = 3.09$$

$$\eta_{T-T} = 0.893 \text{ at } 0.013 \text{ in. } (0.033\text{cm}) \text{ Clearance}$$

Corrected To Standard Air Condition

$$\frac{N}{\sqrt{\theta}_{cr}} = 10,571 \text{ rpm}$$

$$\frac{\dot{W}\sqrt{\theta}_{cr}\epsilon}{\delta} = 6.559 \text{ lbm/sec} \quad (2.975 \text{ kg/sec})$$

$$\frac{\Delta h}{\theta\,cr} = 32.59 \text{ Btu/lbm} \quad (75804 \text{ J/kg})$$

$$P_{R_{T-T}} = 3.371$$

TABLE 2. INTEGRATED 3-D LOSS COMPARISON FOR PHASE II STATOR DESIGN OPTIMIZATION.

Phase II Stator	Configuration	End-Wall Contour	Stack	Loss ($\bar{e}$)
IIA	· 1	Bellmouth (C1)	Baseline	0.068
	2	Inflection (C2)	Baseline	0.056
	3	Bellmouth (C1)	Tangential 20° lean	0.068
IIB	1	Bellmouth (C1)	Baseline	0.053
	2	Large bellmouth (C3)	Baseline	0.062
	3	Large bellmouth (C3)	Compound 13.5° lean	0.055
	*4	Bellmouth (C1)	Compound 26° lean	0.052
	5	Cylindrical	Compound 13.5° lean	0.056
	6	Bellmouth (C1)	Compound 13.5° lean	0.055
	7	Intermediate bellmouth (C4)	Compound 26° lean	0.054

*Final configuration

TABLE 3. COMPARATIVE SUMMARY OF STATOR PERFORMANCE FOR BOTH LART PHASE I AND PHASE II PROGRAMS.

	Low Mach No. Point (0.3)			High Mach No. Design Point (1.06)	
	$\Delta P'/P'$	ω	ω (Analytical)	$\Delta P'/P'$	ω
LART Phase I Model D	0.0038	0.0637	0.0745	0.0337	0.0636
LART Phase II	0.0027	0.0453	0.0520	0.0305	0.0586

TABLE 4. LART PERFORMANCE SUMMARY.

%N/√θ	90			100			110		
$P_{R_{T-T}}$	2.496	3.103	3.539	2.426	3.129	3.564	2.517	3.086	3.508
η_{T-T}	0.893	0.896	0.894	0.892	0.920	0.916	0.887	0.921	0.912
$\Delta h/\theta_{cr}$ (Btu/lbm)[1]	24.62	31.82	36.06	24.92	31.83	35.78	24.63	31.66	35.44
$\dot{W}\sqrt{\theta}_{cr}\epsilon/\delta$ (lbm/sec)[2]	6.599	6.527	6.530	6.591	6.527	6.526	6.472	6.519	6.513
Clearance (in.)[3]	0.014	0.013	0.013	0.013	0.013	0.012	0.013	0.012	0.012

1. J/kg = 2326 × Btu/lbm
2. kg/sec = 0.4536 × lbm/sec
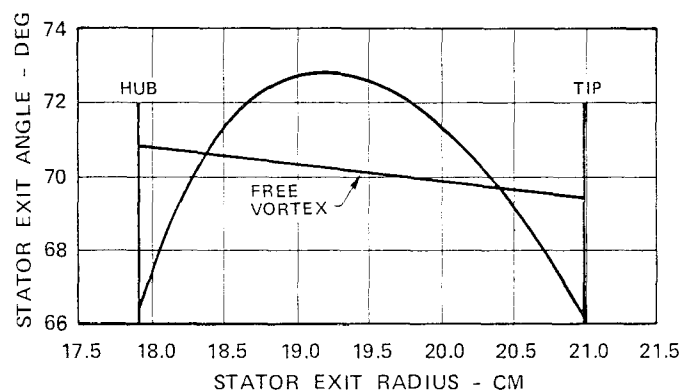3. m = 0.0254 × inch
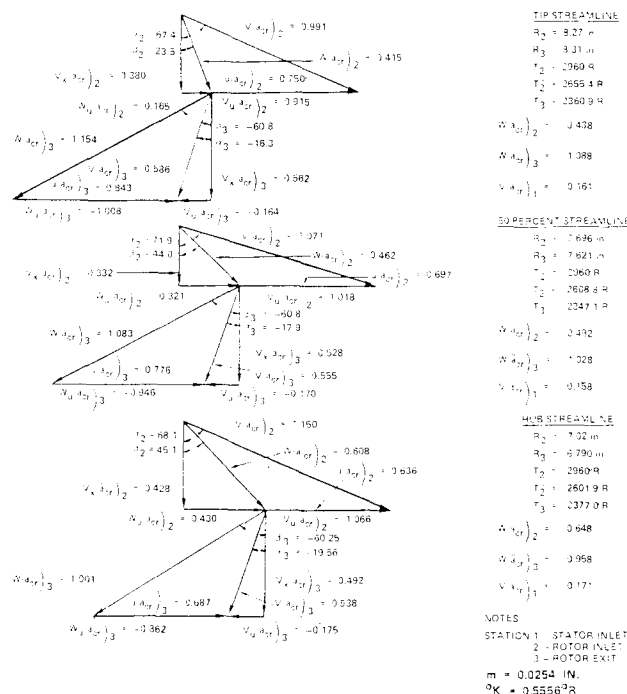

Fig. 1   Stator exit angle distributions

Fig. 2   LART vector diagram

TABLE 5. ROTOR INLET CONDITIONS.

Parameter	Design	Torque Analysis	Axi-Symmetric Analysis (Mass-Averaged Values)
$\Delta P'/P'$	0.0328	0.0323	0.0364
α	70.74	69.52	71.26
β	41.41	35.55	40.59
i	8.74	2.89	7.93
V/V_{cr}	1.076	0.998	1.022
V_x/V_{cr}	0.357	0.352	0.326
V_u/V_{cr}	1.015	0.934	0.968

Fig. 5 Meridional view of Model IIB flow path
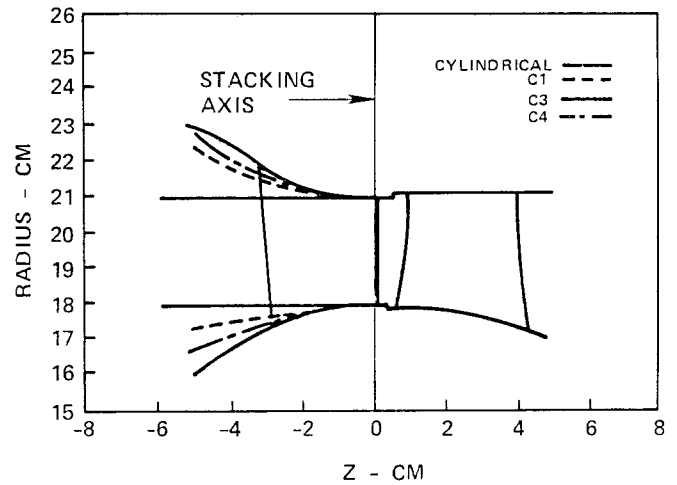

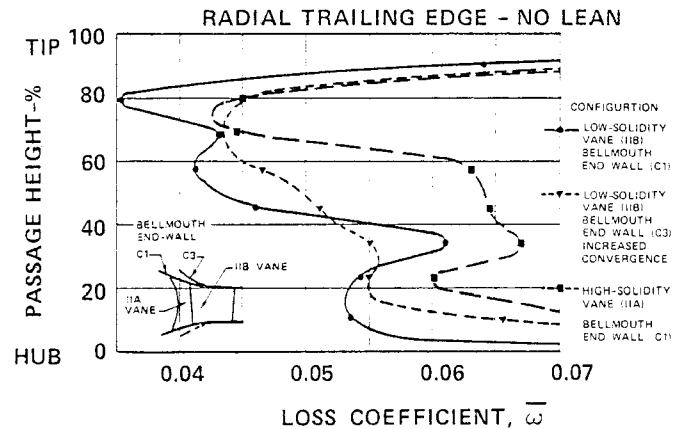Fig. 3 End-wall contours for Model IIA stator

Fig. 6 Effect of end-wall contour and solidity on stator vane losses
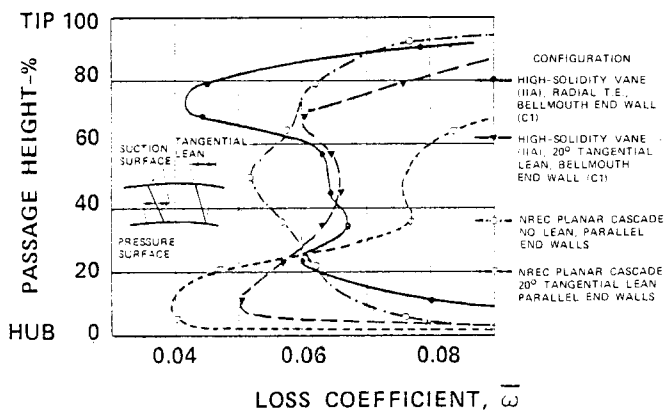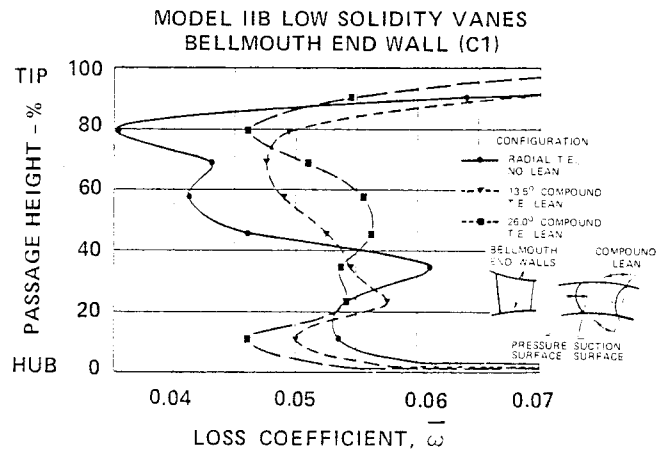

Fig. 4 Effect of tangential lean on stator vane losses

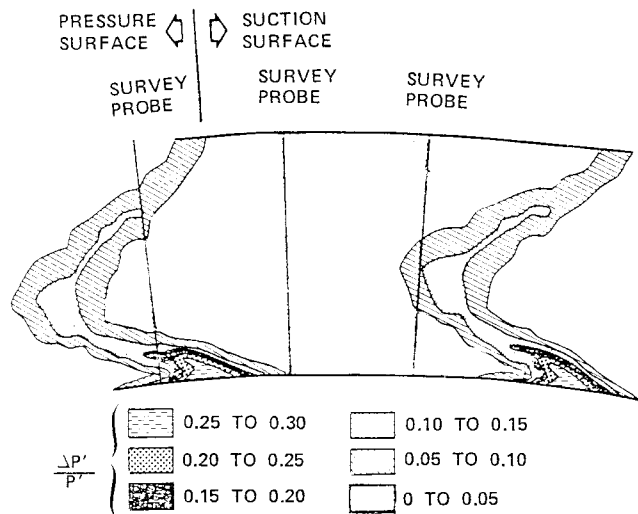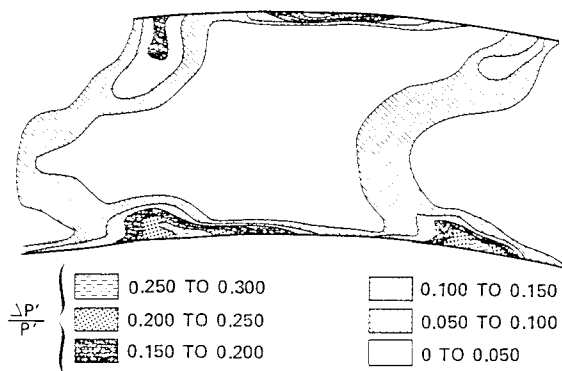Fig. 7 Effect of compound lean on stator vane losses

7

PRESSURE SURFACE ◁ | ▷ SUCTION SURFACE

SURVEY PROBE   SURVEY PROBE   SURVEY PROBE

$\frac{\Delta P'}{P'}$

▨ 0.25 TO 0.30	☐ 0.10 TO 0.15
▦ 0.20 TO 0.25	☐ 0.05 TO 0.10
▧ 0.15 TO 0.20	☐ 0 TO 0.05

Fig. 8 Total pressure loss contours: Phase II stator

$\frac{\Delta P'}{P'}$

▨ 0.250 TO 0.300	☐ 0.100 TO 0.150
▦ 0.200 TO 0.250	☐ 0.050 TO 0.100
▧ 0.150 TO 0.200	☐ 0 TO 0.050

Fig. 9 Total pressure loss contours: Phase I/Model D stator

PRESSURE SURFACE   SUCTION SURFACE

0.60
TIP SECTION

0.56

—×— STAGE TEST DESIGN POINT
0.52
--○-- STATOR TEST DESIGN POINT

DOWNSTREAM REFERENCE PRESSURE RATIO

$\frac{P}{P'_{IN}}$ 0.48

0.48

HUB SECTION

0.44

0.40

0.36
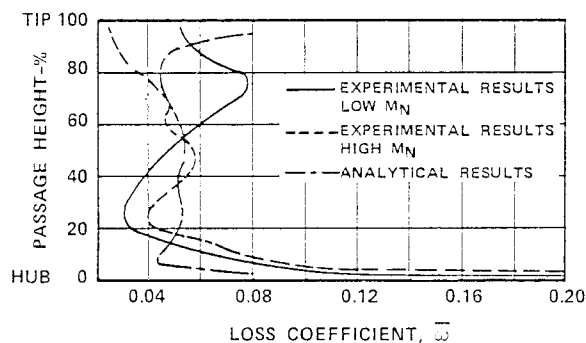
CIRCUMFERENTIAL LOCATION
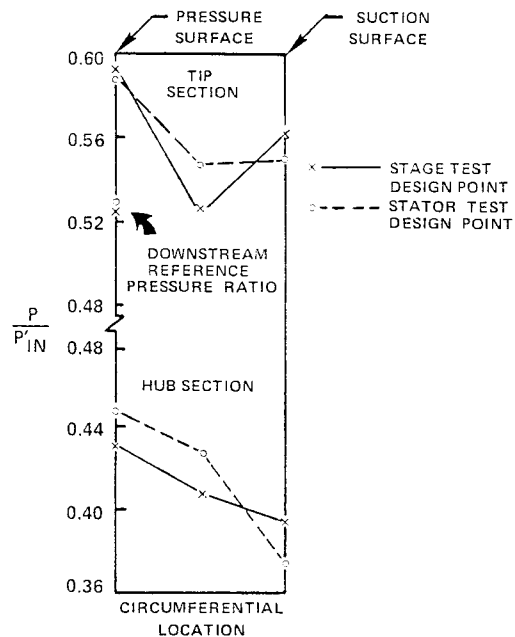
Fig. 11 End-wall pressure distributions measured at the stator trailing-edge plane

TIP 100

PASSAGE HEIGHT–%

80

60

40

20

HUB 0

0.04   0.08   0.12   0.16   0.20

—— EXPERIMENTAL RESULTS LOW M_N
---- EXPERIMENTAL RESULTS HIGH M_N
—·— ANALYTICAL RESULTS

LOSS COEFFICIENT, $\bar{\omega}$

Fig. 10 Radial loss distribution

0.24

0.20

X STATOR SURVEY TOTAL PRESSURE LOSS LEVEL
—— AREA AVERAGED STATIC PRESSURE
0.16
---- UNSCALED PRESSURE TAP

$\frac{\Delta P'}{P'_{IN}}$ 0.12

0.08
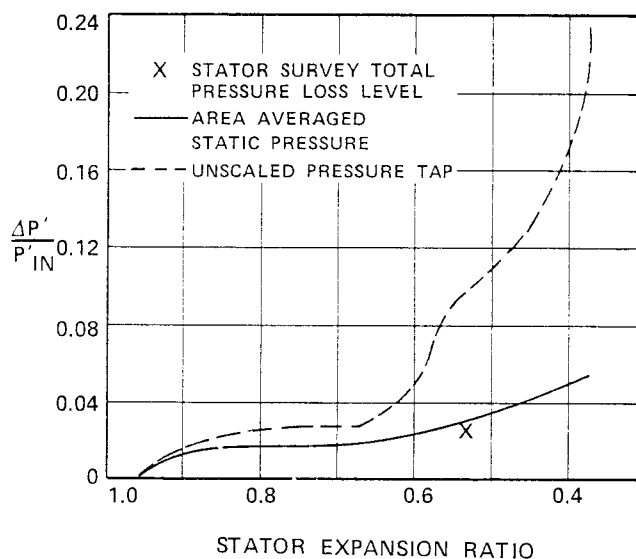
0.04

0

1.0   0.8   0.6   0.4

STATOR EXPANSION RATIO

Fig. 12 Stator total pressure loss computed from baseline stator-reaction test

8